CrystEngComm

Accepted Manuscript

This is an *Accepted Manuscript*, which has been through the Royal Society of Chemistry peer review process and has been accepted for publication.

Accepted Manuscripts are published online shortly after acceptance, before technical editing, formatting and proof reading. Using this free service, authors can make their results available to the community, in citable form, before we publish the edited article. We will replace this *Accepted Manuscript* with the edited and formatted *Advance Article* as soon as it is available.

You can find more information about *Accepted Manuscripts* in the **Information for Authors**.

Please note that technical editing may introduce minor changes to the text and/or graphics, which may alter content. The journal's standard **Terms & Conditions** and the **Ethical guidelines** still apply. In no event shall the Royal Society of Chemistry be held responsible for any errors or omissions in this *Accepted Manuscript* or any consequences arising from the use of any information it contains.

www.rsc.org/crystengcomm

Journal Name

CrystEngComm

ARTICLE TYPE

The first two-fold interpenetrating polyoxometalate-base coordination polymer with helical channels: Structure and catalytic activities

Jing-Quan Sha,[a,b] Long-Jiang Sun,[b] Pei-Pei Zhu[b] and Jianzhuang Jiang[a*]

A polyoxometalate-based coordination polymer with [helix+interpenetration] double configuration feature, $Na[Ag_4(pyttz-I)_2][H_2PMo_{12}O_{40}]$ (POMCP-**1**), was isolated and structurally characterized. POMCP-**1** exhibits the 3D structure with open 3D tunnels along the [10-1], [111], and [1-11] axis. The
10 large void space in the single net induces the interpenetration of the two identical 3D frameworks, resulting in the formation of a highly ordered two-fold interpenetrating aggregate. To the best of our knowledge, this represents the first example of two-fold interpenetrating POMCPs with helical channels. In particular, POMCP-**1** was found to display efficient catalytic activities for the esterification reaction and the photodecomposition of Rhodamine-B.

Introduction

15 Polyoxometalates (POMs), an outstanding class of metal-oxygen clusters with well-defined structure, regular and tunable size, and reversible redox activity have been utilized in many fields such as catalysis, optics, magnetism, and adsorptive applications.[1] Quite
20 recently POMs-based coordination polymers (POMCPs) have emerged as an intriguing class of hybrid crystalline materials, leading to remarkable progress in terms of both the theoretical analysis and practical manipulation.[2] However, the POMCPs with interpenetrating feature have been rarely reported due probably to
25 the big size and uncontrollable coordination geometry of POMs.[3] As a result, design and synthesis of the interpenetrating POMCPs still remains a great challenge in this direction.

On the other hand, the rational synthesis of inorganic-organic hybrid compounds with helical structures is of particular
30 interest due to their importance in optical devices and asymmetric catalysis.[4] However, only a limited number of POMCPs incorporating helical feature have been reported by this group[5] as well as others.[6] Particularly, among the thus far reported POMCPs with helix feature, example with interpenetrating
35 structure has not yet been reported, except for POMCPs with the self-penetrating structure $[Cu_4L_4Mo_6O_{18}(O_3AsPh)_2]$ (L = 1,4-bis(1,2,4-triazol-1-yl)butane).[7] Obviously, novel POMCPs with the [helix+interpenetration] double configuration feature are highly desired in this field since combination of helix and
40 interpenetrating materials is expected to result in novel functionalities from both sides.

As part of our continuous effort in this direction, in the present work the Keggin type ($[PMo_{12}O_{40}]^{3-}$) POMs were selected to construct target coordination polymer with the help of the N-
45 heterocyclic ligands 3-(pyrid-2/3/4-yl)-5-(1H-1,2,4-triazol-3-yl)-1,2,4-triazolyl (hereafter noted H₂pyttz-I, H₂pyttz-II, H₂pyttz-III, respectively), Fig. S1 (ESI)†, as well as the Ag ions, leading to

the isolation of $Na[Ag_4(pyttz-I)_2][H_2PMo_{12}O_{40}]$ (POMCP-**1**). Single crystal X-ray diffraction analysis reveals that POMCP-**1**
50 exhibits an unprecedented two-fold interpenetrating structure with helical feature. In addition, POMCP-**1** shows efficient catalytic activity towards the synthesis of Aspirin and the photocatalytic degradation of Rhodamine-B (RhB), Scheme 1.
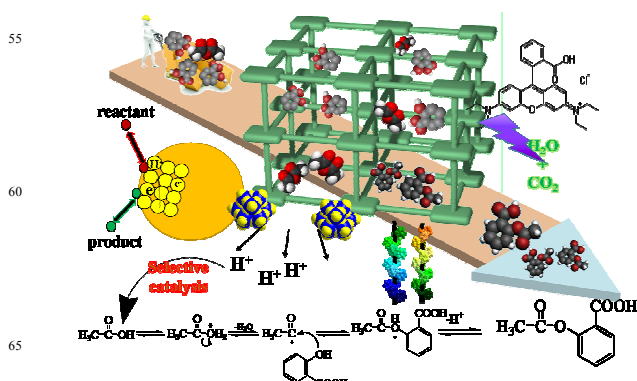
Scheme 1. Schematic representation of POMCP-**1** and the catalytic properties.

Experimental

70 **Materials and General Methods.**
All reagents were commercially available and used without further purification. Elemental analyses (C, H, N) were performed on a Perkin-Elmer 2400 CHN Elemental Analyzer, and Ag was determined with a PLASMA-SPEC(I) ICP atomic
75 emission spectrometer. The IR spectra were obtained on an Alpha Centaurt FT/IR spectrometer with KBr pellet in the 400-4000 cm⁻¹ region. The XRPD patterns were obtained with a Rigaku D/max 2500V PC diffractometer with Cu-Kα radiation, the scanning rate is 4°/s, 2θ ranging from 5-40°. The TG analyses were performed
80 on a Perkin-Elmer TGA7 instrument in flowing N₂ with a heating rate of 10 °C·min⁻¹. The solid diffuse reflectance UV−vis spectra

were recorded on T9 spectrometer of Beijing Purkinje General Instrument Co., Ltd., whereas the UV−vis spectra for solution samples were recorded on a 756 CRT UV-vis spectrophotometer. ^{1}H-NMR and ^{13}C-NMR spectra were recorded on AVANCE-III

5 400MHz. Photocatalytic experiments in aqueous solution were performed in a 500 mL water-cooled quartz cylindrical vessel. Typically, the power of 50 mg was mixed together with 100 ml of 1.0×10^{-5} mol/L (C_0) RhB solution in a beaker by ultrasonic dispersion for 10 min. The mixture was stirred for 0.5 h till

10 reaching the surface-adsorption equilibrium on the particles of the compounds. Then, the mixture was stirred continuously under ultraviolet (UV) irradiation from a 125 W high pressure Hg lamp. At 0, 30, 60, 90, 120,150 min, 3 ml of the sample was taken out from the beaker, respectively, followed by several centrifugations

15 to remove the title compound and a clear solution was obtained for UV-vis analysis.

General procedure for synthesis of Na[Ag$_4$(pyttz-I)$_2$][H$_2$PMo$_{12}$O$_{40}$]. A mixture of H$_3$PMo$_{12}$O$_{40}$ (0.15 mmol, 300 mg), AgNO$_3$ (0.9 mmol, 150 mg), H$_2$pyttz-I (0.2 mmol, 45 mg),

20 and H$_2$pyttz-III (0.2 mmol, 45 mg) was dissolved in 12 mL of distilled water at room temperature, and stirred for 1 h in air. When the pH value of mixture was adjusted to ca.1.84 by 1 M NaOH and the suspension was transferred to an 18 ml Teflon-lined reactor and heated at 170°C for 4 days. After cooling slowly

25 to room temperature, yellow block crystals were filtered, washed with distilled water, and dried at room temperature (35% yield bas4ed on Ag). Elemental analysis: Calcd. For NaAg$_4$C$_{18}$H$_{12}$Mo$_{12}$N$_{14}$O$_{40}$P (2701.17) C 7.99, H 0.44, N 7.25, Ag 15.98%; Found C 7.82, H 0.64, N 7.18, Ag 16.01%.

30 **X-Ray Crystallographic Measurements.** Crystal data for POMCP-**1** were collected on a Bruker SMART-CCD diffractometer with Mo-Kα monochromatic radiation (λ = 0.71069 Å) at 293 K. The structure was solved by the directed methods and refined by full matrix least-squares on F^2 using the

35 SHELXTL crystallographic software package.[8] All the non-hydrogen atoms were refined anisotropically. The positions of hydrogen atoms on carbon atoms were calculated theoretically. The positions of hydrogen atoms were calculated theoretically. The orders "ISOR" and "DFIX" are used to solve the severe

40 disorder problem of Ag2, Na1 and Ag3 atoms. The crystal data and structure refinements of POMCP-**1** are summarized in Table 1. Selected bond lengths and angles are listed in Table S1.

Catalytic synthesis of Aspirin. According to thermodynamics, the esterification reaction is endothermic reaction. As a

45 consequence, the higher reaction temperature is advantageous to the progressing of this reaction. In addition, experiment result indicates that reaction speed is too slow in the temperature lower than 70°C and the yellow product Aspirin can be obtained only in the temperature higher than 90°C. As a total result, in the present

50 case corresponding reaction was carried out in the temperature range of 70-90°C. In detail, 1.5 g of salicylic acid was transferred to a clean, dry three-necked flask with the volume of 50 mL. To which 3.0 mL of acetic anhydride and 0.04 mg of POMCP-1 as catalyst were added. The reaction was then carried out in water

55 bath pot (70-90°C) for a period of time (5-60 min). At 5, 10, 15, 20, 25, 30, 35, 40, 45, 50, 55 and 60 min, 10 μl of sample was taken out from the beaker and diluted with PBS for UV-vis analysis. The content of salicylic acid (SA) and Aspirin (ASP)

were measured by the ultraviolet two-wavelength isoabsorption

60 spectrophotometry due to the high reliability, accuracy, reproducibility, and easiness (ESI)† and Equation 1 and 2).

$$C_{SA} = 40.0166A_{297} - 4.138A_{270} + 0.686 \qquad (1)$$
$$C_{ASP} = 353.25A_{270} - 81.390A_{297} + 7.122 \qquad (2)$$

65 Table 1 Crystallographic and structural refinement data of **1**

Chemical formula	NaAg$_4$C$_{18}$H$_{12}$Mo$_{12}$N$_{14}$O$_{40}$P
CCDC no.	1006550
Formula weight	2701.17
Temperature (K)	293(2)
Wavelength (Å)	0.71069
Crystal system	Monoclinic
Space group	*P 21/c*
a(Å)	14.442(5)
b(Å)	22.524(5)
c(Å)	21.414(5)
α(°)	90.00
β(°)	129.598
γ(°)	90.00
V(Å^3) / Z	5367(3)/4
Density (g·cm^{-3})	3.340
Abs coeff. (mm^{-1})	4.275
F(000)	5016
Data collect θ range	3.26-25.00
Reflns collected	16979
Independent reflns	9421
Rint	0.0292
Data/restraints/parameters	9421/30/847
Goodness-of-fit on F^2	1.063
Final R indices [I > 2δ(I)]	R$_1$ = 0.0557, wR$_2$= 0.1340
R indices (all data)	R$_1$ = 0.0717, wR$_2$= 0.1444
Largest diff. peak and hole(e.$^{-3}$)	3.363 and -2.805

R$_1$ = Σ(||F$_0$|-|F$_c$||)/Σ|F$_0$|, wR$_2$ = Σw(|F$_0$|^2-|F$_c$|^2)^2/Σw (|F$_0$|^2)^2]$^{1/2}$

Results and discussions

70 **Structure description of POMCP-1.**

Single crystal X-ray analysis shows that the asymmetric unit of POMCP-**1** is made up of four Ag ions, one Na ion, two pyttz ligands (L1 and L2), and one {PMo$_{12}$} polyanion, Fig. 1a. There are four crystallographically independent silver centers. The

75 coordination modes of Ag ions, pyttz ligands, and POMs are shown in Fig. S2 (ESI)†. The whole structure of POMCP-**1** can be described as a 3D framework. Firstly, Ag2 ion links with L1 and L2 ligands to form a "T"-type structural unit, which is further extended into the 2D porous CP units with large spaces (19.8 ×

80 11.1Å) *via* Ag1, Ag3, and Ag4 ions, Figs. 1b and S3 (ESI)†. Furthermore, the POMs as four connected building blocks defined by Ag4, Ag4, Ag2, and Ag3 ions are connected to both sides of the CPs like the hanging china lanterns. As a result, a 2D [POMs-CPs-POMs]$_n$ net is obtained, Fig. 1c. Finally, the adjacent

85 2D layers are parallel stacked together forming the 3D structure *via* the short interaction, Figs. 1d and S4(ESI)†.

One fascinating structural feature is that the {PMo$_{12}$} cluster, pyttz (L1 and L2), and Ag ions (Ag1, Ag2, and Ag4) construct left- and right- handed helical chains, Fig.2. More specifically,

90 the left- and right- handed helical chains with a pitch of 22.524 Å

are formed *via* the route of POM-Ag2-L2-Ag1-L1-Ag2-POM-Ag4-POM along *b* axis, which is consistent with the unit length of *b* axis with the value of 22.524(5) Å. Furthermore, the adjacent left-handed and right-handed helical chains are linked in an alternate manner to form a 2D layer with 1D helical channel *via* sharing the POM - Ag1-POM fragments.
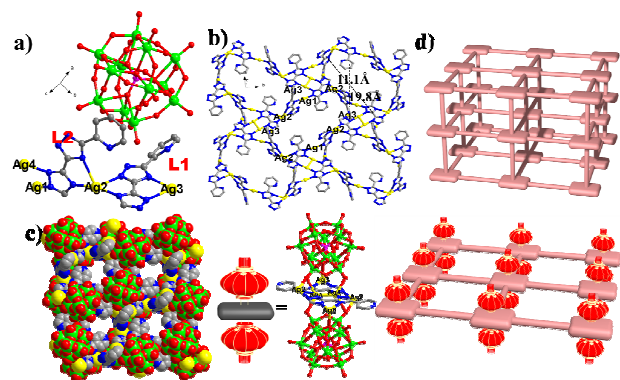
Fig.1. Combined polyhedral/ball/stick and topological representation of (a) the molecular structure unit of POMCP-**1** with all the hydrogen atoms and Na ions omitted for clarity; (b) the 2D CPs; (c) 2D [POMs-CPs-POMs]$_n$ fragment, and (d) 3D POMCPs framework.
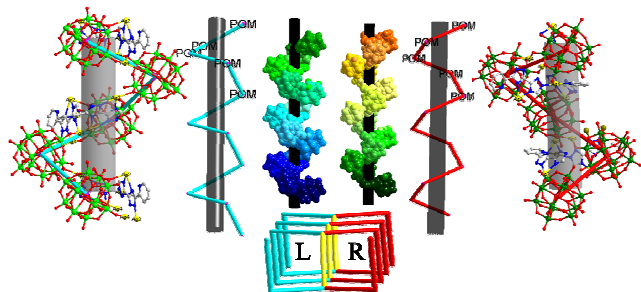
Fig. 2 Combined space-filling and topological representations of left- and right-handed helical chains with all the hydrogen, solvated water molecules, and partly organic molecules omitted for clarity.

Another fascinating structure feature of POMCP-**1** is that the 3D framework possesses the opened 3D tunnels along the [10-1], [111], and [1-11] axis, Figs. 3a-3c. From a topological view point, if we assign the - Ag3 - L1 - Ag2 - L2-, - Ag1 −, -POM-POM- as connectors and POMs as nodes, the 3D framework can be rationalized as a POMCP network with a uninodal 4-connected diamond-like net with 6^6 topology, Fig. 3d. Interestingly, the void space in the single net is so large that two identical 3D frameworks interpenetrate each other to form a highly ordered two-fold interpenetrating aggregate, Figs. 3e and 3f. Because of the interpenetration, the whole structure architecture contains only small cavities, only 1.54 % of the cell volume calculated by PLATON.

For the purpose of comparison, the structural features for a series of POMCPs constructed from POM and PYTTZ[5] obtained previously are also listed in Table S2 (ESI)†. It seems that the rigid plane spacer between two triazolyl rings and the radiate coordination style of the pyttz ligand supports the formation of helical channels. More specifically, the rigid plane and the twisted V-shaped coordination modes of L-1 and L-2, Ag ions, and POMs together lead to the formation of helical channels in POMCP-**1**, Fig. 4a, verifying the synthetic strategy. In comparison with Na$_2$[Ag$_6$(pyttz-II)$_2$(H$_2$O)][PMo$_{12}$O$_{40}$]·(OH)[5c] (POMCP-**2**) and [Ag$_3$(Hpyttz-III)$_2$][H$_2$PMo$_{12}$O$_{40}$][5e] (POMCP-**3**), we find that the pore size of 2D CPs becomes larger due to the introduction of the PYTTZ-I (ca.8.4 Å to 10.7 Å to 17.59 Å), which leads to the increase in the distance among the POMs (12.62×13.62Å), Fig. 4b. On the other hand, the asymmetrical coordination mode of POMs produces the imbalance of the electronic cloud distribution. As a result, the distance of the adjacent 2D layers with POMs becomes larger, amounting to ca.13.57 Å. Both effects contribute in a quite positive manner for the formation of interpenetrating structure. Finally, because the pore size of subunit of POMCP-**1** is larger than the diameter of POMs (10 Å), two identical 3D frameworks with helix interpenetrate each other to form a highly ordered two-fold interpenetrating aggregate, Figs. 4c and 4d.
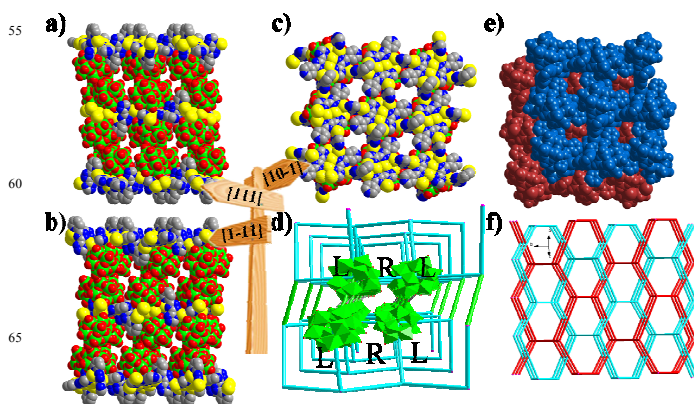
Fig.3. Space-filling models (a, b, c) and topology (d) showing the POMCPs with three directional tunnels and helical structure, and two-fold interpenetrating structures (e and f).
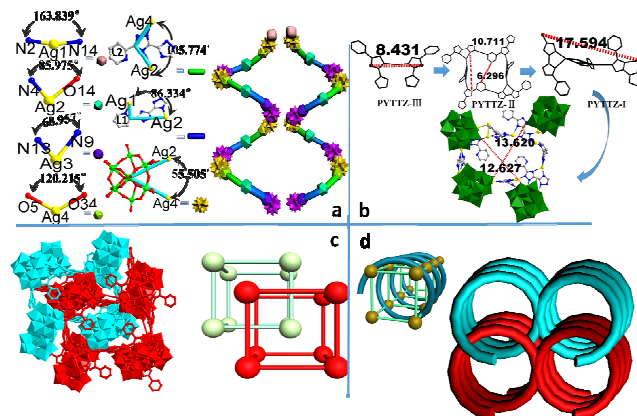
Fig. 4 Representation of the coordination mode of each building block and the contribution to the formation of the helical structure (a); the subunit of 2D CPs with the larger pore due to the introduction of the ligand PYTTZ-I (b), and the combined polyhedral/stick (c) and schematic view (d) of the [helix+interpenetration] subunits (c) and (d).

FT-IR, XRPD, TG, ^{1}H-NMR and ^{13}C-NMR Characterization
The IR spectrum of POMCP-**1** is shown in Fig. S5 (ESI)†. Characteristic bands at 1055, 964, 881 and 773 cm^{-1} are attributed to ν (P-O), ν (Mo=O), and ν (Mo-O-Mo) vibrations, respectively. Bands in the region of 1644-1163 cm^{-1} are attributed to the pyttz ligand. In particular, the IR characteristic bands of POMCP-**1** before and after catalysis match well, indicating that the structure

of POMCP-**1** does not change. The XRPD pattern for the POMCP-**1** is presented in Fig. S6 (ESI)†. The diffraction peaks in simulated and experimental patterns match well, indicating the good phase purity of POMCP-**1**. The difference in reflection intensities between the simulated and experimental patterns is due to the different orientation of the crystals in the powder samples. The thermal analysis of POMCP-**1** is shown in Fig. S7 (ESI)†. The total loss of 15.74% in the range of 40-620℃, agrees with the calculated weight loss of 15.77%, corresponding to the loss of PYTTZ of per formula. These results further confirm the formulas of POMCP-**1**.

The IR spectra of catalysate and Aspirin standard are shown in Fig. S8 (ESI)†. Characteristic bands in the region of 3000-2500 cm^{-1} are attributed to ν (-COOH), while those at 1755 and 1684 cm^{-1} to ν (-C=O) of ester and carboxylic acid, and 1300 and 1182 cm^{-1} to ν (C-O) of ester and carboxylic acid, respectively. ^{1}H-NMR and ^{13}C-NMR are shown in Fig. S9 (ESI)†. ^{1}H-NMR δ: 2.343 (s, 3H,-CH$_3$), 7.137 (s, 1H,-CH), 7.348 (s, 1H,-CH), 7.616 (s, 1H,-CH), 8.119 (s, 1H,-CH), 11.185 (s, 1H,-COOH); ^{13}C-NMR δ: 21.02 (-CH$_3$), 122.27-151.29 (Ar-C), 169.76 (C=O), 170.17 (-COOH). These results indicate that the catalysate is Aspirin and the phase purity is good.

Optical energy gap

The UV−vis absorption spectrum of POMCP-**1** was measured in the crystalline state at room temperature, Fig. S10(ESI)†. The energy bands from 200 to 300 nm may be assigned to the pπ (O terminal) → dπ*(Mo) electronic transitions in the Mo=O bonds and dπ-pπ-dπ electronic transitions between the energetic levels of the Mo-O-Mo bonds, respectively.[9]

In order to explore the conductivity of POMCP-**1**, the measurements of diffuse reflectivity for powder samples were used to explore their band gaps (Eg), which are determined as the intersection point between the energy axis and the line extrapolated from the linear portion of the adsorption edge in a plot of the Kubelka–Munk function F against E.[10] The optical absorption related to Eg values can be assessed from the steep absorption edge at 2.3 eV, Fig. S11 (ESI)†, which shows the presence of optical band gaps and the nature of semiconductivities. As a result, POMCP-1 would be a kind of potential photocatalyst.

Photocatalysis properties

The use of POMs as photocatalysts to decompose waste organic molecules so as to purify the water resources has attracted great attention in recent years.[11] The introduction of transition-metal complexes as functional groups into POMs can enrich their potential applications. Herein, to investigate the photocatalytic activities of POMCP-**1** as catalyst, the photodecomposition of RhB is evaluated under UV light irradiation through a typical process. The photodegradation of RhB assisted by POMCP-**1** and their matrix ((NBu$_4$)$_3$[PMo$_{12}$O$_{40}$]) is shown in Fig. 5. It can be seen that the photocatalytic decomposition rate, defined as 1-C/C$_0$, is 75.98% for POMCP-**1** and 34.12% for the matrix after 150 min of irradiation. Obviously, the degradation rate of POMCP-**1** under UV light is higher than the matrix. Additionally, compared with POMCP-**3**,[5e] the photocatalytic activity of POMCP-**1** is also higher. Generally, the POM subunit is regarded as the photocatalytic active component for the POMCPs. As a consequence, the photocatalytic activities for the POMCPs are mainly dependent on their POM-containing structures. More

specifically, the 3D helical framework is filled by building blocks leaving only small cavities (0.4 % of the cell volume calculated by PLATON) in POMCP-**3**. However, in POMCP-**1** the asymmetrical polar modification and the helical structure prohibit well the conglomeration and deactivation of POMs, allowing the enhancement of their catalytic properties. On the other hand, the enhanced photocatalytic property may be arisen from the TMCs acting as photosensitizer under UV light, which promotes the transition of electrons to POMs.
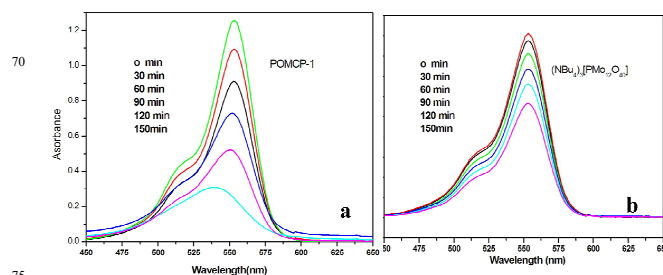
Fig. 5 UV–vis adsorption changes observed for RhB solution as a function of UV light irradiation time in the presence of POMCP-1 as catalyst (a) and (NBu$_4$)$_3$[PMo$_{12}$O$_{40}$] as catalyst (b).

Catalytic activity analyses of Aspirin.

As mentioned above the esterification reaction is endothermic reaction and the increase in the reaction temperature is advantageous to the reaction progressing. Fig. 6 and Table S3 (ESI)† show the influence of reaction temperature on the catalytic synthesis of Aspirin. Keeping the same reaction time, the higher the temperature is, the higher the conversion rate of salicylic acid is. So are the reaction yield of Aspirin and the selectivity of catalyst. However, the increasing trend of three physical quantities becomes slowly along with the temperature rising after 40 min. The influence of reaction time on the catalytic synthesis of Aspirin is shown in Fig. 7 and Table S3 (ESI)†. The result shows that the conversion rate of salicylic acid, the yield of Aspirin, and the selectivity of catalyst are significantly enlarged with increasing the time during the initial period of 5-40 minute from the very beginning, which change to be not significantly dependent on the time after the conduction of reaction after 40 min. In addition, when the reaction temperature is higher than 90°C, the yield of Aspirin changes in an irregular manner, which may be due to the occurrence of the side effects. Taking into account the cost as well as the energy and efficiency, the reaction time of 40 min and the temperature of 80°C were employed, resulting in the conversion rate of salicylic acid of 93.85%, the yield of Aspirin of 81.43%, and the selectivity of catalyst of 86.79%. In addition, POMCP-**1** could be readily isolated from the reaction mixture by simple filtration. The filtered catalyst was washed by 95% ethanol and dried, and then employed for the following subsequent run of catalysis experiment. The result indicated little fall in the catalytic activity, Fig. S12 (ESI)†, revealing that the POMCP-**1** catalyst is stabilized and can be recycled and effectively reduce the cost.

Reaction kinetics analyses

In order to quantitatively understand the reaction kinetics for the synthesis of Aspirin by using POMCP-**1** as catalyst, the reaction rate equation model is set up to obtain the rate constant (κ) and reaction order (n)

$$r_{SA} = d\ C_{SA}/dt = \kappa\ C_{SA}^{\ n}\quad (1)$$

$$\ln(dC_{SA}/dt) = \ln\kappa + n\ln C_{SA} \quad (2)$$

where C_{SA} is the concentration of the salicylic acid aqueous solution for different time of UV illumination and t is the time, respectively. For the test condition, herein $dC_{SA}/dt \cong \triangle C_{SA}/\triangle t$. According to eqn (2), if $[-\ln(\triangle C_{SA}/\triangle t)]$ is plotted as a function of $\ln C_{SA}$, a straight line should be obtained whose slope is n (min^{-1}) and intercept is $\ln\kappa$. Fig. 8 shows the reaction kinetics analysis at 80°C, the κ and n values are 0.0990 and 1.8224, respectively. And the correlation coefficient (R) also shows good statistics values. Then the rate equation is obtained as detailed bellow:

$$r_{SA} = 0.099 \, C_{SA}^{1.8224} \quad (3)$$

In a same way, the κ values are obtained as 0.0344, 0.0618, 0.0990, 0.3463 at 70, 75, 80, 85°C, respectively. Finally, the apparent activation energy of the reaction by using POMCP-**1** as catalyst was calculated to be 113.49 KJ.mol^{-1}.
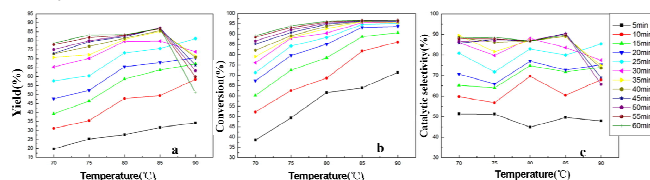
Fig. 6 Catalytic activity of POMCP-**1** *vs* the reaction temperature: (a) Yield of Aspirin *vs* temperature; (b) Conversion of salicylic acid *vs* temperature; and (c) Catalytic selectivity *vs* temperature.
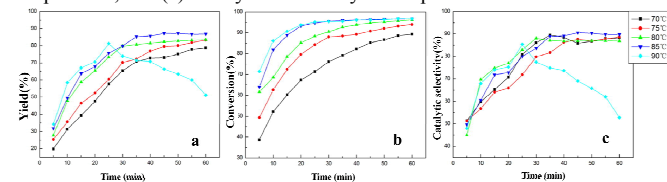
Fig.7 Catalytic activity of POMCP-**1** *vs* the reaction time: (a) Conversion of salicylic acid *vs* time; (b) Yield of Aspirin *vs* time; and (c) Catalytic selectivity *vs* time.
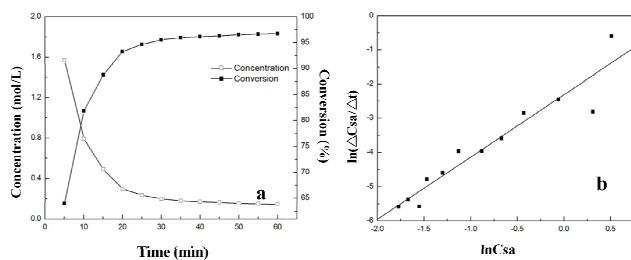
Fig. 8 Concentration and conversion change of salicylic acid with time (left) and the linear relation of ln ($\triangle C_{SA}/\triangle t$) with $\ln C_{SA}$ at 80°C.

The possible mechanism of the catalytic synthesis of Aspirin is shown in Scheme II. As we all know, the catalytic synthesis of Aspirin is essentially an acid catalytic reaction. According to the rate equation, we deduce that the reaction between carbonyl cation and salicylic acid is the key step. As a consequence, large electronegativity on the POM surface can stabilize carbocation intermediate, which is favor of the offensive of hydroxyl oxygen on the SA, promoting effectively the generation of the product Aspirin, similar to the steric effect. Additionally, the charges of POMs in POMCP-**1** are non-localized, and hydroxy proton exhibits strong liquidity in the POM surface and high acidity, which plays a key role during the pseudo-liquid phase catalytic behavior of POMs. Finally, the reactant molecules can fully enter

the interior POMCP-**1** crystals and fully contact the catalytic activity center during the initial reaction phase, which is in favor of catalytic activity of the catalyst. Along with the extension of time, the conversion rate of salicylic acid molecules tend to be balanced, while the yield of the Aspirin maintains in a certain range.
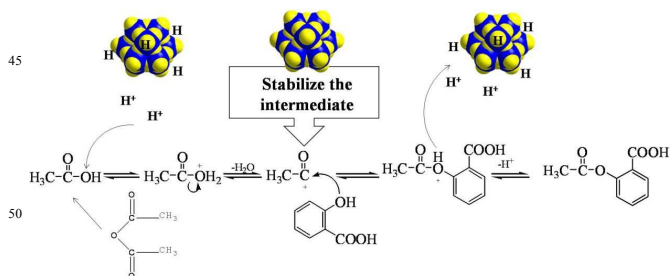
Scheme II. The suggested reaction mechanism for the synthesis of Aspirin.

Conclusions

In summary, a novel polyoxometalate-based coordination polymer with the [helix+interpenetration] double configuration feature has been synthesized under hydrothermal condition. In particular, this polyoxometalate-based coordination polymer possesses good catalytic activity towards the synthesis of Aspirin and the photocatalytic degradation of RhB, revealing the great potential application of various kinds of novel POMCPs in the field of catalysis.

Notes and references

[a] Beijing Key Laboratory for Science and Application of Functional Molecular and Crystalline Materials, University of Science and Technology Beijing, Beijing 100083, China

[b] The Provincial Key Laboratory of Biological Medicine Formulation, School of Pharmacy, Jiamusi University, Jiamusi, 154007, P. R. China

† Electronic Supplementary Information (ESI) available: [Crystallographic data and CCDC can be obtained free of charge from the Cambridge Crystallographic Data Centre via www.ccdc.cam.ac.uk/data_request/cif. Tables of selected bond lengths (Å), bond angles (deg) and Figures, IR, XRPD for compound and the experimental sections are provided in supporting information.]. See DOI: 10.1039/b000000x/

1. (a) A. Müller, F. Peters, M. T. Pope and D. Gatteschi, *Chem. Rev.*, 1998, **98**, 239; (b) C. L. Hill, *Chem. Rev.*, 1998, **98**, 1; (c) A. Dolbecq, E. Dumas, C. R. Mayer and P. Mialane, *Chem. Rev.*, 2010, **110**, 6009; (d) S. G. Mitchell, C. Streb, H. N. Miras, T. Boyd, D. L. Long and L. Cronin, *Nat. Chem.*, 2010, **2**, 308; (e) Z. M. Zhang, S. Yao, Y. G. Li, H. H. Wu, Y. H. Wang, M. Rouzières, R. Clérac, Z. M. Su and E. B. Wang, *Chem. Commun.*, 2013, **49**, 2515.

2. (a) C. Y. Sun, S. X. Liu, D. D. Liang, K. Z. Shao, Y. H. Ren and Z. M. Su, *J. Am. Chem. Soc.,* 2009, **131**,1883; (b) S. T. Zheng, J. Zhang, X. X. Li, W. H. Fang and G. Y. Yang, *J. Am. Chem. Soc.*, 2010, **132**, 15102; (c)

J. Song, Z. Luo, D. K. Britt, H. Furukawa, O. M. Yaghi, K. I. Hardcastle and C. L. Hill, *J . Am. Chem. Soc.,* 2011, **133**, 16839; (d) L. Zhou, J. Liu, W. B. Ji, H. Huang, H. L. Hu, Y. Liu and Z. H. Kang, *J. Mater. Chem. A.,* 2014, **2**, 12686; (e) R. Li, X. Q. Ren, J. S. Zhao, X. Feng, X. Jiang, X. X. Fan, Z. G. Lin, X. G. Li, C. W. Hu and B.Wang, *J. Mater. Chem. A.,* 2014, **2**, 2168; (f) D. Y. Du, J. S. Qin, S. L. Li, Z. M. Su and Y. Q. Lan, *Chem. Soc. Rev.,* 2014, **43**, 4615; (g) X. L. Wang, Z. H. Chang, H. Y. Lin, A. X. Tian, G. C. Liu, J. W. Zhang and D. N. Liu, *CrystEngComn.,* 2015, **17**, 895.

3. (a) Z. M. Zhang, Y. G. Li, W. L. Chen, E. B. Wang and X. L. Wang, *Inorg. Chem.Commun.*, 2008, **11**, 879; (b) L. L. Fan, D. R. Xiao, E. B. Wang, Y. G. Li, Z. M. Su, X. L. Wang and J. Liu, *Cryst.Growth Des.*, 2007, **7**, 592; (c) H. X. Yang, G. L. Li, B. Xu, T. F. Liu, Y. F Li, R. Cao and S. R. Batten, *Inorganic Chemistry Communications*, 2009, **12**, 605.

4. (*a*) O. M. Yaghi, *Nature*, 1999, **402**, 276; (*b*) O. M. Yaghi, *J. Am. Chem. Soc.*, 1998, **120**, 8571; (*c*) B. Q. Ma, D. S. Zhang, S. Gao, T. Z. Jin, C. H. Yan and G. X. Xu, *Angew. Chem., Int. Ed.*, 2000, **39**, 3644; (*d*) M. Sasa, K. Tanaka, X. H. Bu, M. Shiro and M. Shionoya, *J. Am. Chem. Soc.*, 2001, **123**, 10750; (*e*) L. Han, H. Valle and X. H. Bu, *Inorg. Chem.*, 2007, **46**, 1511; (*f*) B. Ding, Y. Y. Liu, X. X. Wu, X. J. Zhao, G. X. Du, E. C. Yang and X. G. Wang, *Cryst. Growth Des.*, 2009, **9**, 4176.

5. (a) P. P. Zhang, J. Peng, J. Q. Sha, A. X. Tian, H. J. Pang, Y. Chen and M. Zhu, *CrystEngComm.,* 2009, **11**, 902; (b) J. Q. Sha, M. T. Li, J. W. Sun, P. F. Yan, G. M. Li and L. Zhang, *Chem. Asian J.,* 2013, **8**, 2254; (c) J. Q. Sha, M. T. Li, J. W. Sun, Y. N. Zhang, P. F. Yan and G. M. Li, *Dalton Trans.*, 2013, **42**, 7803; (d) J. W. Sun, M. T. Li, J. Q. Sha, P. F. Yan, C. Wang, S. X. Li and Y. Pan, *CrystEngComm.*, 2013, **15**, 10584; (e) M. T. Li, J. Q. Sha, X. M. Zong, J. W. Sun and P. F. Yan, *Cryst. Growth Des.*, 2014, **14**, 2794.

6. (a) R. Kawamoto, S. Uchida and N. Mizuno, *J. Am. Chem. Soc.*, 2005, **127**, 10560; (b) S. Uchida, R. Kawamoto, H. Tagami, Y. Nakagawa and N. Mizuno, *J. Am. Chem. Soc.*, 2008, **130**, 12370; (c) H. Y. An, E. B. Wang, D. R. Xiao, Y. G. Li, Z. M. Su and L. Xu, *Angew. Chem. Int. Ed.*, 2006, **45**, 904; (d) S. T. Zheng and G. Y. Yang, *Dalton Trans.*, 2010, **39**, 700; (e) C. J. Zhang, H. J. Pang, Q. Tang, H. Y. Wang and Y. G. Chen, *Inorg. Chem. Commun.*, 2011, **14**, 731; (f) X. L. Wang, J. Li, A. X. Tian, D. Zhao, G. C. Liu and H. Y. Lin, *Cryst. Growth Des.*, 2011, **11**, 3456; (g) H. Fu, C. Qin, Y. Lu, Z. M. Zhang, Y. G. Li, Z. M. Su, W. L. Li and E. B. Wang, *Angew. Chem. Int. Ed.,* 2012, **51**, 7985.

7. B. Liu, J. Yang, G. C. Yang and J. F. Ma, *Inorg. Chem.*, 2013, **52**, 84.

8.(a) G. M. Sheldrick, SHELXS–97, Program for Crystal Structure Solution, University of Göttingen, Germany, 1997. (b) G. M. Sheldrick, SHELXL–97, Program for Crystal Structure Refinement, University of Göttingen, Germany, 1997.

9. (a) M. T. Pope, Heteropoly and Isopoly Oxometalates; Springer-Verlag: Berlin, 1983. (b) B. Liu, Z. T. Yu, J. Yang, W. Hua, Y. Y. Liu and J. F. Ma, *Inorg. Chem.*, 2011, **50**, 8967.

10. (a) J. I. Pankove, Optical Processes in Semiconductors; Prentice Hall: Englewood Cliffs, NJ, 1971. (b) W. M. Wesley and W. G. H. Harry, Reflectance Spectroscopy; Wiley: New York, 1966.

11. (a) M. Y. Dong, Q. Lin, H. M. Su, D. Chen, T. Zhang, Q. Z. Wu and S. P. Li, *Cryst. Growth Des.*, 2011, **11**, 5002; (b) X. L. Wang, Z. H. Chang, H. Y. Lin, A. X. Tian, G. C. Liu, J. W. Zhang and D. N. Liu, *RSC Adv.*, 2015, **5**, 14020; (c) H. Zhang, J. H. Lv, K. Yu, C. M. Wang, C. X. Wang, D. Sun and B. B. Zhou, *Dalton Trans.*, 2015,**44**, 12839; (d) K. Yu, H. Zhang, J. H. Lv, L. H. Gong, C. M. Wang, L. Wang, C. X. Wang and B. B. Zhou, *RSC Adv.*, 2015, **5**, 59630.

1

The first two-fold interpenetrating polyoxometalate-base coordination polymer with helical channels. Structure and catalytic activities

Jing-Quan Sha,[a,b] Long-Jiang Sun,[b] Pei-Pei Zhu,[b] and Jianzhuang Jiang[a*]

[a] *Beijing Key Laboratory for Science and Application of Functional Molecular and Crystalline Materials, University of Science and Technology Beijing, Beijing 100083, China*

[b] *The Provincial Key Laboratory of Biological Medicine Formulation, School of Pharmacy, Jiamusi University, Jiamusi, 154007, P. R. China*

A polyoxometalate-based coordination polymer POMCP-**1** with [helix+interpenetration] double configuration was successfully isolated, which shows effective catalytic activities for the esterification reaction and the photodecomposition of Rhodamine-B.